2001

# Feasibility study of online high-spatial-resolution MOSFET dosimetry in static and pulsed x-ray radiation fields

Anatoly B. Rosenfeld
*University of Wollongong*, anatoly@uow.edu.au

M. L. Lerch
*University of Wollongong*, mlerch@uow.edu.au

T. Kron
*Mater Hospital, Newcastle*

E. Brauer-Krisch
*European Synchrotron Radiation Facility, France*

A. Bravin
*European Synchrotron Radiation Facility, France*

*See next page for additional authors*

# Feasibility Study of Online High-Spatial-Resolution MOSFET Dosimetry in Static and Pulsed X-Ray Radiation Fields

Anatoly B. Rosenfeld, *Senior Member, IEEE*, Michael L. F. Lerch, *Member, IEEE*, Tomas Kron, Elke Brauer-Krisch, Alberto Bravin, Andrew Holmes-Siedle, *Senior Member, IEEE*, and Barry J. Allen

***Abstract*—Improvements have been made in the measurement of dose profiles in several types of X-ray beams. These include 120-kVp X-ray beams from an orthovoltage X-ray machine, 6-MV Bremsstrahlung from a medical LINAC in conformal mode and the 50–200 keV energy spectrum of microbeams produced at the medical beamline station of the European Synchrotron Radiation Facility. Using a quadruple metal–oxide–semiconductor field-effect transistor (MOSFET) sensor chip in "edge on" mode together with a newly developed sensor readout system, the feasibility of online scanning of the profiles of quasi-static and pulsed radiation beams was demonstrated. Measurements of synchrotron pulsed microbeams showed that a micrometer-scale spatial resolution was achievable. The use of several MOSFETs on the same chip gave rise to the correction of misalignments of the oxide films of the sensor with respect to the microbeam, ensuring that the excellent spatial resolution of the MOSFET used in "edge-on" mode was fully utilized.**

## I. Introduction

THE radiation microbeam is a useful technique in microelectronic device testing applications. Heavy-ion microbeams are often used in single-event upset (SEU) studies [1] because they can target single nodes of interest in an integrated circuit. The microelectronics industry has dramatically reduced (to submicrometer size) the scale of p-n junctions and metal–oxide–semiconductor field-effect transistor (MOSFET) structures and the photon beams used in pattern generation [2]. Techniques of beam dosimetry must follow these developments. In the present case, we explore the possibilities of a soft X-ray/EUV detector with very small dimensions. Because of the use of thin films in an "edge-on" mode, we can obtain detectors of width on the order of 0.1 $\mu$m and thus detect the profiles of microbeams of the same order. This has potential in the fields of microbeam radiotherapy and photolithography [3], [4].

At the European Synchrotron Radiation Facility (ESRF) in France and at the Brookhaven National Laboratory (BNL) in the United States, a microbeam radiation therapy (MRT) program exists to investigate the potential of this alternative radiation therapy method [6]–[8]. At ESRF, the current MRT program uses a multislit collimator capable to produce microbeams of variable thickness up to 50 $\mu$m width with a peak-to-peak interval of 210 $\mu$m [9]. The correct dose measurements of such microbeams demand an excellent spatial resolution of a detector system. This is a challenge, since ionization chambers and photodiodes with micrometer-sized apertures and adequate responses are difficult to engineer.

Another field of radiation dosimetry that requires a method incorporating high spatial resolution for dose mapping is conformal radiation therapy with megavolt photons produced by a LINAC for intensity modulated radiation therapy (IMRT) [10] or the gamma knife using Co-60 gamma rays [11]. Quality assurance (QA) of quasi-static radiation fields demands the use of a scanning dosimetry system with a spatial resolution of 500 $\mu$m or better. The above techniques involve very steep dose gradients so that the dosimetric profile must be highly resolved. Existing online scanning systems use ionization chambers or photodiodes with typical spatial resolutions of $\sim$3–4 mm. This is not good enough for the modern requirements of IMRT.

Research in this field started with the investigation of microbeams of X-rays and high-intensity synchrotron radiation, applied to the response of single, small MOSFET structures [2], [3]. In [2], the irradiation was done with a beam perpendicular to the gate oxide plane. This method can be used for individual calibration of MOSFET dosimeters on a wafer (chip). The response is calculated using the calibration curve $\Delta V_{\rm th} = f(D)$ obtained for a precisely similar MOSFET under a standard, broad radiation beam. Here $\Delta V_{\rm th}$ is change in threshold voltage and $D$ is ionization kerma in Gray or rad($SiO_2$); see e.g., [4]. The question of radical improvement in spatial resolution by the use of "edge-on" MOSFETs was proposed and tested by Rosenfeld *et al.* [3]. In that work, a manual setup was tested with synchrotron radiation and 200-$\mu$m spaced X-ray beams with widths of $\sim$30 $\mu$m. It was shown that the Ukrainian n-MOSFET detector gave good resolution using beams at the National Synchrotron Light Source (NSLS), BNL. Although the sensor was in a steel (TO-18) package, a beam profile with 1-$\mu$m resolution was demonstrated. More recent Monte Carlo simulations using the EGS4 code (see Fig. 9) demonstrate the good agreement between the simulated and experimental results. A perspex phantom with a detector at a depth of 5 mm was used. The metal (TO-18 without lid) packaging of the n-MOSFET

Manuscript received July 17, 2001. This work was supported by NHMRC and DIST under Grants.

A. B. Rosenfeld and M. L. F. Lerch are with the Centre for Medical Radiation Physics, University of Wollongong, 2522 Wollongong, NSW, Australia (e-mail anatoly@uow.edu.au).

T. Kron is with Mater Hospital, Newcastle, Australia.

E. Brauer-Krisch and A. Bravin are with the Installation Européenne de Rayonnement Synchrotron (ESRF), F-38043 Grenoble Cedex, France.

A. Holmes-Siedle is with REM Oxford Ltd., OX29 4PD Oxford, UK.

B. J. Allen is with St. George Cancer Care Centre, Sydney, Australia.

Publisher Item Identifier S 0018-9499(01)10644-1.

did not produce significant strong dose enhancement or scattering even with the low-energy X-rays in question. However, further improvement was required to improve the orientation of the MOSFET in the beam and to substitute a material of lower $Z$ as the substrate. In particular, any misalignment must be minimized, as it will affect the absolute accuracy of the spatial resolution.

Thus, the aim of this work is to develop and test an online micrometer-scanning computer-controlled MOSFET dosimetry system with improved spatial resolution. The system was intended to be applicable to quasi-static and pulsed radiation fields and able to measure total dose as well as a dose-rate profile suitable for beam quality assurance and real-time patient dosimetry.

## II. Online MOSFET Dosimetry System

### A. Overall Dosimetric System

Radiation dosimetry with MOSFET detectors is a well-known method that has been successfully applied in space dosimetry [12] and, more recently, in radiation medicine. The advantage of this detector is in the small-sized dosimetric volume and the ability of multiple readout without erasing information of the accumulated dose in the process. Usually a MOSFET detector is operated in an integral mode, where the dose is determined from the shift in the threshold voltage before and after it is irradiated. In this case, the effect of a fading and/or a temperature error can be significant if a long time occurs between irradiations or the temperature changes between the initial and final readout. Dose measurement is especially important during radiation therapy, where the typical dose for one fraction is $\sim$100–150 rads and an accuracy of better than 2% is required. The important issues that should be addressed in the optimization of the MOSFET dosimetry system are as follows:

1) online measurement in a wide dynamic range of accumulated dose and dose rate;
2) possibility of scanning in an online capacity, similar to a diode system;
3) good spatial resolution, preferably better than 0.2 mm;
4) online measurements in a pulsed mode with consecutive dosimetry for each pulse;
5) possibility of avoiding temperature and fading error;
6) possibility of compensation of the effect of sublinearity of the MOSFET detector.

A MOSFET dosimetry system that addresses most of these issues has been developed at the Centre for Medical Radiation Physics at the University of Wollongong, Australia, and is shown in Fig. 1. The system employs an integrated MOSFET with two types of p-MOSFET on the same chip, designed and produced by REM Oxford, U.K. [12]. The REM low-$Z$ chip carriers used were designed specifically for use with low-energy photons. The developed system reads ten MOSFETs sequentially online in a short time, and the results are sent via an RS232 link to a PC, where, using specially developed software, they are saved to disk and presented graphically within seconds. The current MOSFET reading can also be seen on the LCD display and sequenced by manual override.

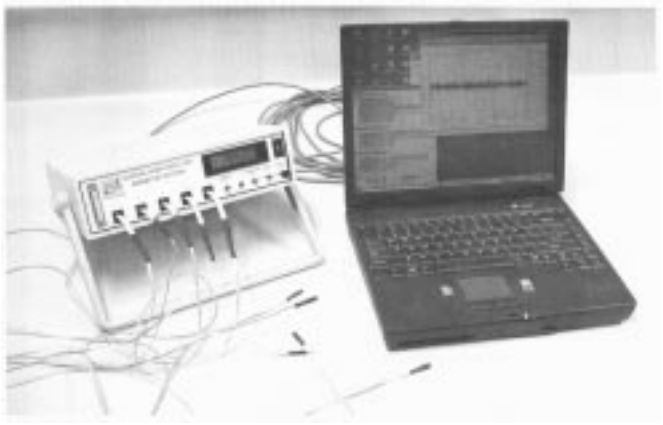

Fig. 1. The online MOSFET dosimetry system designed and built by the Centre for Medical Radiation Physics, University of Wollongong, Australia.

The internal microprocessor unit that performs the "simultaneous" readout allows one to use both MOSFET detectors in active mode. In the current model, the K-type and R-type MOSFETs are operated with a gate bias voltage of $+12$ and $+5$ V, respectively. The software and internal microprocessor corrects for any drift of the MOSFET threshold voltage due to slow border states induced by radiation or thermal effects [13].

Pulses generated by the remote-controlled beam shutter triggered the data acquisition (DAQ) system. A 20-m cable connected the reader in the control room to the exposure hutch. After each radiation pulse, a DAQ program displayed consecutive steps in the threshold voltage of the RADFETs during the mechanical scan across the microbeam image. A control run of the reader–sensor system, after installation at ESRF, demonstrated background stability of better than $\pm 2$ mV.

### B. Software and Display Presentation

Special software, MosPlot 4.1, was designed using MATLAB for making profiles in quasi-static and pulsed radiation beams. In the former mode, the user presets the readout period. In pulsed applications, an external transistor–transistor logic (TTL) pulse from the beam control system triggers the MOSFET readout system. The software allows for the online graphical presentation of the change in $V_{\rm th}$ or increments of $\Delta V_{\rm th}$ for consecutive readouts, i.e., dose-rate measurements. The period between each readout of all the MOSFET detectors is user selected ($\geq$0.5 s). It should be noted that the actual readout time of each MOSFET (duty time) is much less than the time between two consecutive readouts. Correction of sublinearity of a MOSFET, or a lookup library for the conversion of data into absorbed dose, can be implemented.

### C. Compensation of Thermal Error

Compensation of the thermal error $\Delta V_{\rm th}/\Delta T$ is an important issue in MOSFET dosimetry and limits its use at low doses. One approach is based on the use of dual identical MOSFETs on the same source substrate that are irradiated with different gate biases applied [14]. In readout mode, the $\Delta V_{\rm th}$ from both MOSFETs are subtracted. Assuming that both MOSFETs have

the same temperature coefficient $\Delta V_{\mathrm{T}}/\Delta T$, then the dose response should be independent of temperature.

Another approach of thermal stabilization is to use a thermostable point on the $I_{\mathrm{sd}}$ versus $V_{\mathrm{gs}}$ characteristic [15], where $\Delta V_{\mathrm{th}}/\Delta T = 0$ and reading out corresponding current. However, with accumulation of dose, the thermostable point on the $I_{\mathrm{sd}}$ versus $V_{\mathrm{gs}}$ characteristic shifts. Thus the original corresponding readout current no longer necessarily guarantees a thermostable dose response. Another shortcoming of this approach is the spread of MOSFET thermostable points even within one batch of devices, which then demands adjustment of the corresponding thermostable current value for each MOSFET. Using MOSFETs with different gate-oxide thicknesses on the same chip does not allow one to minimize the thermal error for both MOSFETs due to an excessively different thermostable readout current.

Our approach is independent of the type of MOSFET (p or n), the oxide thickness, the gate bias, and the accumulated dose. Fig. 2 shows the change of $V_{\mathrm{th}}$ versus temperature readout simultaneously with dose-rate response $\Delta V_{\mathrm{th}}$ versus temperature for each MOSFET (R- and K-type) on the same chip without any irradiation. The measurements were done under a constant flow of hot air using the same readout current for both MOSFETs. The format of the MosPlot 4.1 data acquisition software is shown. The filled circles in Fig. 2 clearly demonstrate the significant change in $V_{\mathrm{th}}$ versus temperature of $\sim$50 mV for the R-type and $\sim$20 mV for the K-type that would introduce a thermal error of 10 and 40 rads, respectively, over the 20 K range. The different sign of slopes on these two curves shows that the thermostable points are different for different MOSFET geometries.

The data points in Fig. 2 related to $\Delta V_{\mathrm{th}}$ (open circles) show no trend up or down versus temperature over a range of at least 20 K. The observed fluctuation in the measured $\Delta V_{\mathrm{th}}$ is almost entirely the result of statistical fluctuation in the ADC. This stability is sufficient for the measurement of a dose of $\sim$0.2 rad (a genuine shift of 1 mV in the R-type FETs) and can probably be extended to 0.05 rad by refining the ADC and increasing the gate bias during irradiation.

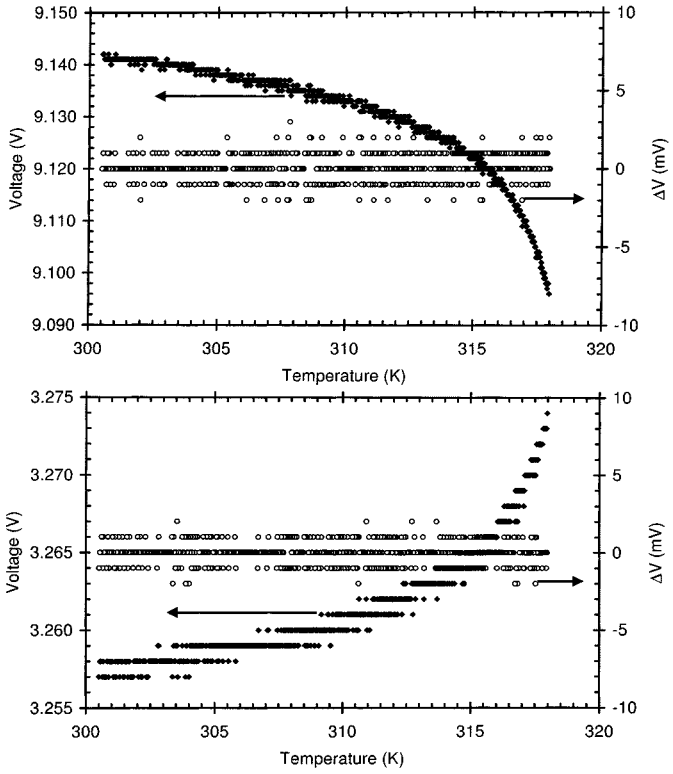


Fig. 2. Control experiment without radiation, showing the changes versus temperature of the measured, absolute threshold voltages $V_{\mathrm{th}}$ (filled circles) and the "dose signal" $\Delta V_{\mathrm{th}}$ (open circles) provided by the CMRP-designed reader system. Shown for the two types of p-MOSFET on the REM Type TOT502 (top figure) thick oxide, Type R and (bottom figure) thin oxide, type K. No temperature-related trend is evident in the $\Delta V_{\mathrm{th}}$ data, only ADC noise.

### *D. Scanning With an Online MOSFET*

The spatial resolution of the silicon diodes and ionization chambers currently used in clinical beam-checkers is on the order of 6 mm. Reducing the volume of the sensing devices simply increases the problems caused by the very low currents generated. Theoretically, it is possible to improve the sensitivity of the diode by increasing the reverse bias (increasing of depletion layer). However, it is not practical due to the significant degradation of the signal-to-noise ratio through the increase of reverse dark current.

We now consider the requirements needed for the online scanning MOSFET system to map profiles of radiation fields that incorporate penumbras with steep dose gradients. In this mode, the MOSFET must be able to measure the dose-rate change versus coordinate rather than integral dose. Fig. 3 shows the change of the dose rate in arbitrary units versus the $X$ coordinate leading to a penumbra with width $X_{\mathrm{p}}$ for a continuous

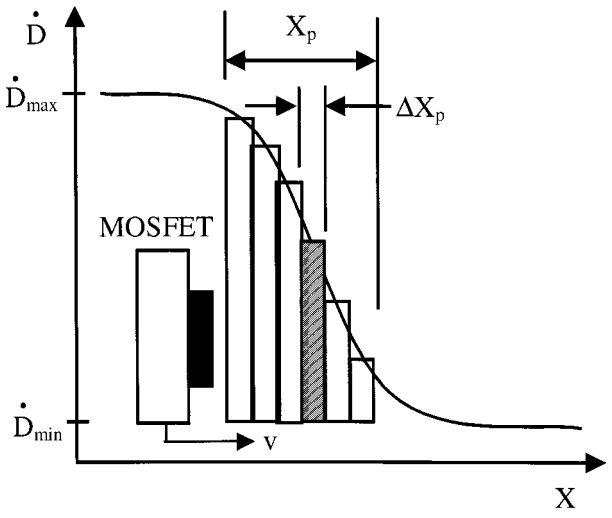


Fig. 3. Schematic representation of a penumbra dose rate versus distance. The width of the penumbra is $X_p$ and the spatial resolution of the MOSFET sensor is $\Delta X_p$.

radiation field. Assume that an "edge-on" MOSFET [3] is continuously moving across a penumbra with speed $v$, followed by readout with period $T$. Such measurements will lead to an integrated dose for each step of $\Delta X_{\mathrm{p}}$, i.e., $\Delta V_{\mathrm{th}} = V_{\mathrm{th,\,i+1}} - V_{\mathrm{th,\,i}}$.

The shaded area of each increment represents the relative dose accumulated for each step and is proportional to the

average dose rate for any particular step. The condition of penumbra measurements is defined as follows:

$$\frac{D_{\min}(\text{MOSFET})}{\dot{D}} < T < \frac{X_{\text{p}}}{v} \tag{1}$$

where $D_{\min}(\text{MOSFET})$ is the minimal detectable dose with the MOSFET in integral mode, $\dot{D}$ is the average dose rate, $T$ is the readout period, $X_{\text{p}}$ is the penumbra width (see Fig. 3), and $v$ is the speed of the MOSFET scanner.

Another limit that will be applicable is $T \gg t_{\text{r}}$, where $t_{\text{r}}$ is the readout time. For example, in radiation therapy where the average $\dot{D}$ is ~10 rad/s, $D_{\min}(\text{MOSFET}) \sim 1$ rad and $v \sim 0.1$ mm/s (scanning diode system used in a water tank), it means that $0.1 < T < 10$ s for a penumbra of 1 mm. For such a penumbra, $T = 1$ s, it is possible to get ten points with an average $\Delta V_{\text{th}} \sim 50$ mV/step. The readout period $T = 1$ s also well satisfies the condition $T \gg t_{\text{r}}$ for online systems ($t_{\text{r}} \sim 0.2$ ms). In the same radiation field with $T = 0.2$ s, it is possible to measure the penumbra with an accuracy of 20 $\mu$m. Note that even 20-$\mu$m steps do not represent the lower step size limit due to the intrinsic spatial resolution of the "edge-on" MOSFET.

Additionally, in contrast to the diode, the MOSFET sensitivity can be adjusted by changing the gate bias. In the case for $T = 20$ ms and a MOSFET sensitivity of 25 mV/rad ($V_{\text{g}} \sim 60$ V) for a used R-type MOSFET, it is theoretically possible to make penumbra measurements with $X_{\text{p}} \sim 20$ $\mu$m with a step size of ~4 $\mu$m.

### *E. Quadruple MOSFET Detector*

Our improved microbeam dosimetry approach is based on the use of a quadruple X-ray detector. Fig. 4 shows a scanning electron micrograph (SEM) image of the bare chip and the direction of the X-ray beam. This is the REM type TOT502 RADFET, a quadruple MOSFET chip with dimensions $1 \times 1 \times 0.5$ mm$^3$. Two MOSFETs, Q1 and Q4 (type R), have gate-oxide thickness values of about 0.9 $\mu$m, and two, Q2 and Q3 (type K), have thickness values of about 0.15 $\mu$m. The dosimeter sensors for this experiment were selected for preirradiation stability. The chip carrier selected (Type CC6) was a thin 0.2-mm glass-epoxy board with ten surface-mountable leads. The chip was encapsulated in opaque epoxy. On the axis of the microbeam, the thickness of epoxy was less than 2 mm.

For the ESRF experiment, chip carrier CC3 was used. This is a thin glass–epoxy carrier ("chip-on-board" technology) with 14 pins ($7 + 7$), which will connect with a standard DIL socket, in which the sensor is cantilevered so that a buildup cap can be placed around the chip. The normal built-in encapsulation is a hemisphere of opaque epoxy resin.

The package was mounted in "edge-on" mode on a movable computer-controlled stage in the experimental hall. The initial alignment with the beam is described above but initial dose measurements led to a refined alignment. For high-energy photons, the sensor region was mounted inside a small block of Perspex $9 \times 9 \times 12$ mm$^3$—a "buildup cap" that created electronic equilibrium. The R-type RADFETs were irradiated under a +5 V gate bias and the K-type under a +12 V gate bias. These irradiation bias values were found to give the best linearity of threshold voltage versus dose. As the response curve rolls off slightly with accumulated dose, linearity was checked under different radiation pulse duration times.

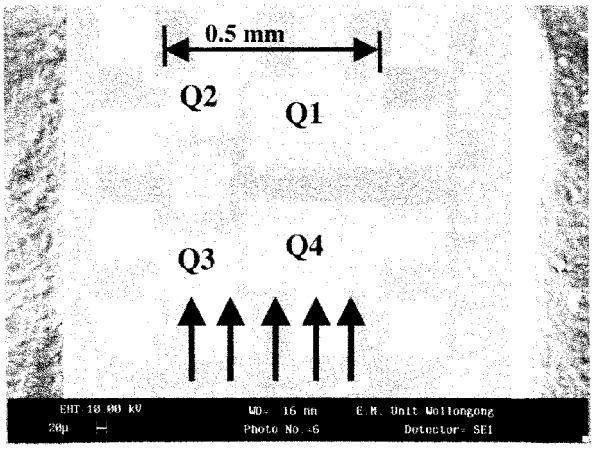


Fig. 4. SEM of the REM TOT500 RADFET chip, showing the four RADFETs, Q1–Q4. Also shown is the "edge-on" geometry for the experiments described in this paper. The radiation beam impinges on the edge of Q3 and Q4.

## III. Radiation Facilities

### *A. Penumbra of a 120-kV$_p$ X-Ray Beam*

The performance of the online MOSFET dosimetry system in scanning mode was tested on a 120-kV$_{\text{p}}$ X-ray field from a Siemens Stabiliplan 2 orthovoltage irradiation unit. Fig. 5 illustrates the irradiation geometry. The "edge-on" MOSFET detector was mounted on a Wellhoefer beam-scanning device in air, running at a velocity of 0.1 mm/s. Only one R-type and one K-type MOSFET were connected in this series of experiments. In the case of 120-kV$_{\text{p}}$ X-ray radiation, the average range of secondary electrons is less than 10 $\mu$m, so that the built-in encapsulation was adequate to provide charged-particle equilibrium. The 120-kV$_{\text{p}}$ superficial beam chosen as the lateral range of the secondary electrons is on the order of 10 $\mu$m and does not contribute significantly to a widening of the penumbra. The beam has a half-value layer of 3-mm Al and a focal spot size of approximately 7 mm in diameter at the anode. The beam was collimated by an $8 \times 8$ cm$^2$ metal applicator with a 2-mm perspex front window. A 2-mm-thick lead sheet was placed at 30 cm distance from the focal spot to create a sharp beam edge. The penumbra was scanned in both directions (from beam to out of beam and reverse) at a distance of 0.5 cm from the lead sheet.

Assuming that the edge of the lead sheet does not introduce additional penumbra broadening, one can calculate the penumbra width from the focal spot size, the focus-to-lead sheet distance (30 cm), and the lead sheet-to-detector distance. For the distance chosen (0.5 cm), it would be 0.1 mm. Respectively, the exact shape of the penumbra depends on the actual shape of the focal spot.

### *B. LINAC With Multileaf Collimator*

A Varian 21EX medical linear accelerator was run in 6-MV *bremsstrahlung* mode. The Wellhoefer scanning holder was used under a 120-leaf Varian multileaf collimator (MLC) [16], at a distance of 55 cm from the target. The secondary jaws were set to a field size of $36 \times 36$ cm$^2$ and the leaves of the

MLC were fully closed. As shown in Fig. 6(b), the Tungsten leaves of the collimator are rounded at their tips. Adjacent leaves have a tongue-and-groove design to minimize radiation leakage [Fig. 6(c)]. The focus-to-detector distance (FDD) was 100 cm. Scans were performed in two directions, as illustrated in Fig. 6(a):

Direction A) parallel to the leaves/under a leaf;
Direction B) orthogonal to the leaves/under a closed set of leaves.

Only one R-type and one K-type MOSFET were connected in this series of experiments. The layout of the chip with two R-type and two K-type MOSFETs can be seen in Fig. 4. For 6-MV *bremsstrahhlung*, the built-in encapsulation was not adequate to provide charged-particle equilibrium. The absolute response of the MOSFET in free-air geometry per (average) monitoring unit (MU) would be reduced. Usually 1 MU $=$ 1 rad (TE) under conditions of electronic equilibrium. For this, 6-MeV X-rays require about 15 mm of buildup.

### C. Synchrotron Microbeam Radiation Facility

MRT is carried out on ESRF's Medical Beamline, ID17.[1] The energy for this experiment was 5 GeV at a current of up to 200 mA and an electron lifetime of about 50 h. The setup used was identical to the normal MRT configuration, but the normal energy of the electron beam is at 6 GeV, thus not corresponding to the same wiggler spectrum and consequently microbeam spectrum used for MRT irradiations. The source of radiation is a 21-pole 150-mm period wiggler magnet in the storage ring, which has a 1.5-T magnetic field. The average energy of the X-rays produced is 100 keV. The primary components for the MRT beam are in an optics hutch about 30 m away from the source. At the ESRF, the current MRT program uses the multislit collimator in a configuration producing about 25-$\mu$m-wide beams with a spacing of 210 $\mu$m. The MRT fast shutter can work with exposure times down to as low as 10 ms. The minimum opening time was chosen for the experiment in order to avoid saturation of the detector. The mechanical stage, to which the "edge-on" MOSFET detectors were mounted, was a computer-controlled goniometer with a minimum step size of 5 $\mu$m. The intensity of the beam was monitored by an ionization chamber before and after the collimator and the stage. Careful alignment was applied by the use of lasers and gafchromic films and with the help of slits in order to exactly identify the microbeam measured by the MOSFET detector.

## IV. Experimental Results and Discussion

### A. X-Ray 120-kV$_p$ Beam and LINAC

In both experiments (X-ray orthovoltage machine and MLC LINAC), the R-type MOSFET was selected due to the requirement defined by (1). Fig. 7 illustrates the results of online simultaneous measurements of integrated dose and dose-rate profile (penumbra) obtained with the MOSFET dosimetry system in scanning mode. The RS232 of the battery-operated ten-channel MOSFET reader was connected to the PC via a 7.5-m cable, and the lead lengths of the MOSFET probe were 1 m.

[1]More details of the facility can be found at www.esrf.fr.

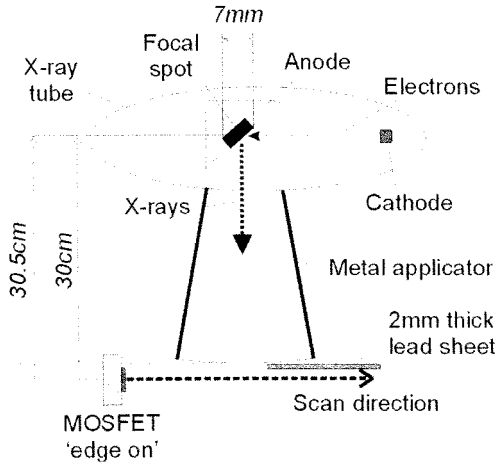


Fig. 5. Penumbra formation of the Siemens X-ray machine.

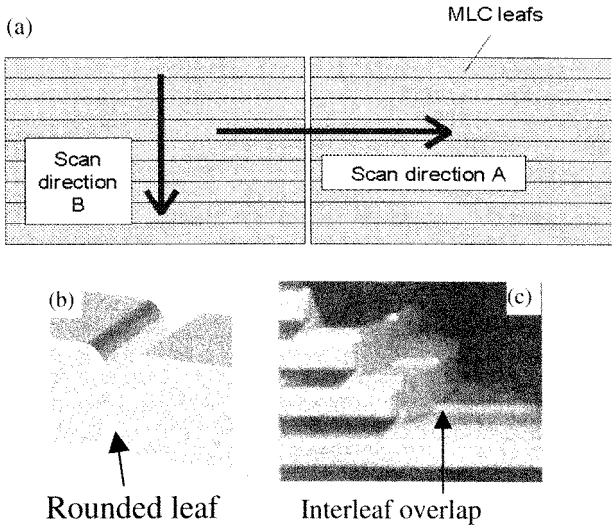


Fig. 6. Various views of the Varian multileaf collimator. (a) Two scan directions of the MOSFET relative to the top view of the MLC. Scan direction A is to investigate adjacent leaf radiation leakage. Scan direction B is to investigate stop-gap leakage due to the curved tips of the leaves. In (b) and (c), it is emphasized how the radiation leakage may arise.

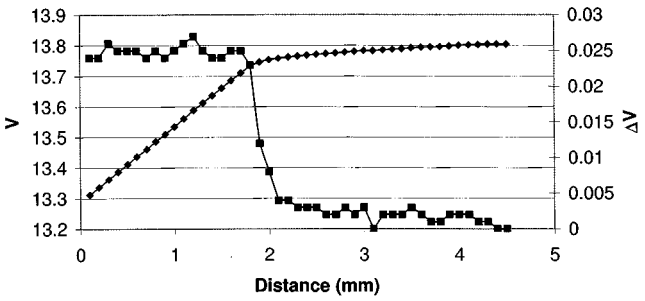


Fig. 7. Online measurement with an "edge-on" TOT500 RADFET of the penumbral profile formed by a lead plate in the beam of 120-kV$_p$ X-rays, using the setup shown in Fig. 5.

It is possible to see that the dose rate distribution is flat outside and under the lead filter and the penumbra had a width (between the 10% and 90% level) of about 100 $\mu$m. This agrees with the operators' estimate of a 0.1-mm penumbra, based on the focal spot size and geometry of the experiment. The distance between

the MOSFET and lead sheet was 0.5 cm. The beam profiles in orthogonal scanning directions were in good agreement.

Fig. 8 illustrates a similar result with the leaves of MLC closed. The two curves represent the change in the cumulative dose on the RADFET ($V_{\rm th}$) derived dose-rate distribution ($\Delta V$) along and between two leaves [see Fig. 6(a)—scan direction A]. Also presented is the averaging curve for $\Delta V_{\rm th}$ mode for a readout exposure period of 3 s for the same MOSFET.

The ratio of the gradients of the integral dose curve ($V_{\rm th}$) measured under the rounded tips defining the central axis of the beam (position of the maximum response on the $\Delta V$-curve) and 8 mm outside of this point (flat part of the $\Delta V$ curve is $\sim 9:1$. This value is in good agreement with data obtained from the exposure of film dosimeters, indicating about 2% radiation leakage outside of the central beam axis and 17–18% at the point of maximum leakage under the point where the rounded tips meet [see Fig. 6(b)]. A similar ratio of the radiation leakages under the MLC leaves on the central axis to off-axis of the beam was obtained from the $\Delta V_{\rm th}$ versus $X$-curve in Fig. 7 (the smoothed curve). In this case, it was 15/1.7 or about 8.8.

The penumbra of the radiation leakage field, measured under the rounded tips, of the left and right leaf of the collimator was symmetrical and of width of about 1 mm. The noise of $\pm 1$ mV in the dosimeter readout signal $\Delta V$ mode corresponds to the resolution of the ADC used in this version of the MOSFET readout system when scanning in the orthogonal direction of the central axis of the beam.

It was not possible to measure radiation leakage resulting from the tongue-groove effect with the same "edge-on" probe due to the much smaller penumbra and lower intensity in comparison with the radiation leakage under tips and leaves. Equation (1) suggests that for this online scanning measurement, an increase in the sensitivity of the MOSFETs (increasing of gate bias of 50 V) together with a reduction of $T$ of up to 0.5 s is required.

These experiments have demonstrated the characterization of quasi-static and continuous radiation fields in routine radiotherapy facilities. Such characterization is particularly interesting for dose planning and dose verification in IMRT using a medical LINAC.

### *B. Synchrotron Microbeams*

Fig. 9 shows a comparison of the results of "edge-on" n-MOSFET detector with EGS4 simulation for a 30-$\mu$m single microbeam in a perspex phantom at depth 5 mm [17]—results taken at NSLS, BNL [3]. The metal (TO-18 without lid) packaging of the n-MOSFET did not demonstrate a significant effect of dose enhancement or scattering from the metal substrate for this low-energy X-ray synchrotron beam.

Fig. 4 shows an SEM image of the multiple RADFET (REM TOT500) adopted to improve alignment. It also shows the direction of the photon beam in this experiment. Devices Q3 and Q4, RADFETs with differing gate-oxide thickness values, face the edge-on beam. Crude alignment and equilibrium questions were discussed above for the 100-kV X-ray case. The reader was controlled by a TTL trigger pulse generated at ESRF immediately after the beam shutter was closed. The four RADFET channels from the TOT500 sensor were connected to the reader situated

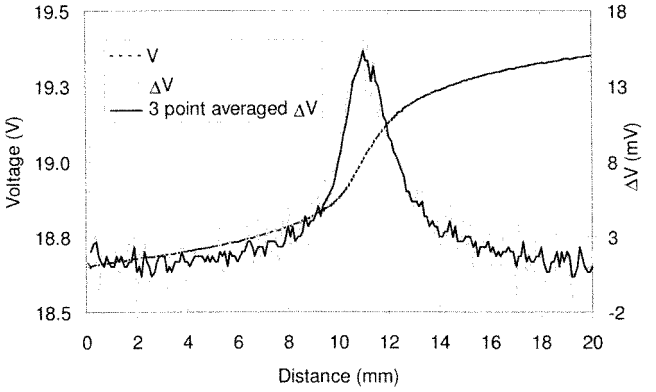


Fig. 8. Measured stop-gap radiation leakage of the Varian multileaf collimator, scanned with an "edge-on" TOT500 RADFET. The scan direction was as in Fig. 6(a) (scan direction A). Note that the R-type RADFET used here received a total radiation dose to cause a $V_{\rm th}$ shift of 10 000 mV prior to this experiment and is still giving good results.

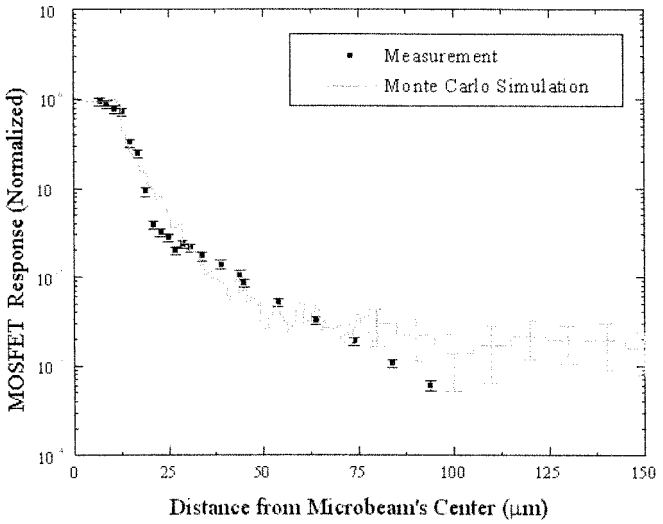


Fig. 9. A comparison with an EGS4 simulation of a measured "edge-on" n-MOSFET profile for a 30-$\mu$m single microbeam of "white" X-rays from NSLS, BNL [17].

in the control room by 20 m of cable. The software displayed the consecutive changes in the threshold voltage of each RADFET after each radiation pulse following a scanning step across the radiation microbeam.

The four RADFETs (within 0.5 mm of each other) were read after each exposure. Linearity of the RADFET response was checked under different radiation duration times. The step length of the translation measurements across the microbeams was 5 $\mu$m, and typical exposure times were 10 ms.

Figs. 10 and 11 show the response of RADFET R (Q4), chip #101, for selected radiation microbeams #11 and #22 of the microbeam array generated in this experiment. The electron energy was 5 GeV and currents were 154 and 198 mA, respectively. The full-width at half-maximum for both peaks was the same, about 35 $\mu$m. The minimum dose between two peaks (valley dose) was found as expected at a distance of 100 $\mu$m away from a peak dose.

Fig. 12 shows the normalized response of Q3 and Q4 RADFETs on the same chip during the scan of beam #22. All

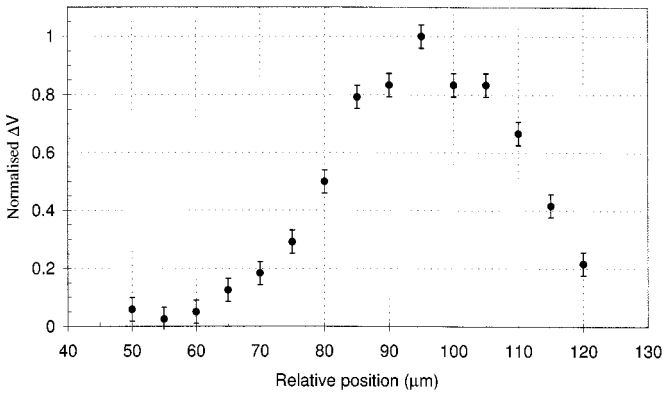


Fig. 10. Profile of radiation microbeam no. 11 measured with an "edge-on" TOT500 RADFET type R.

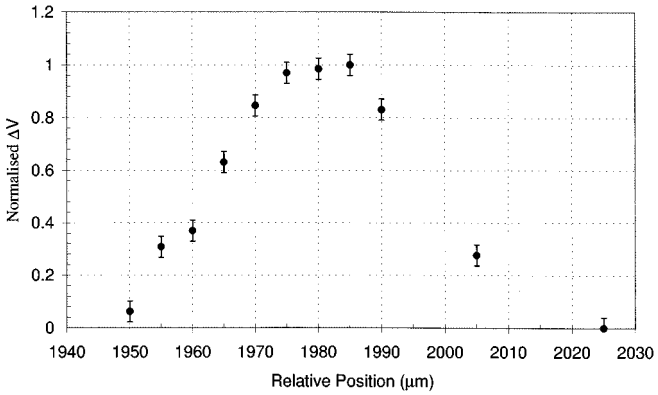


Fig. 11. Profile of radiation microbeam no. 22 measured with an "edge-on" TOT500 RADFET, using the identical RADFET, subsequent to measuring beam number 11, Fig. 10).

RADFETs were measured after the radiation exposure for each RADFET position on the radiation microbeam. The response of both RADFETs demonstrated that they both are aligned within the 0.5-mm height of the microbeam array (see beam layout, Fig. 4). Total change in $V_{\rm th}$ of each RADFET was less than 1000 mV, which ensures that we are still in the linear response range on the total-dose scale of the RADFET.

From Fig. 12, one can see that the peak in the response of Q1 relative to Q4 is shifted by about 20 $\mu$m. One should also note the high spatial resolution achieved. A geometrical calculation suggests that the chip was tilted at an angle of about 5.7°. It is very useful to know the degree of misalignment, as this result can be used for precise alignment of the chip with the radiation microbeam. A goniometer on movable stage can be used to bring the two peaks into line. Accurate overlapping of curves indicates that RADFETs are in the ideal "edge on" mode. More accurate beam profile measurements, with the best possible spatial resolution of the RADFET, may be possible. Similar arrangements can be done for K-type RADFETs Q3 and Q2.

Using the dual sensitivity RADFETs in the same chip allows one to measure the P/V ratio with higher accuracy by using the R-type sensor in a valley and K-type in a peak region. It will avoid any nonlinearity effect associated with the large dynamic range of doses such as those used in MRT and where the P/V ratio is extremely important for QA and possibly for the precise measurement of the dose deposited in the tissue. The DAQ time

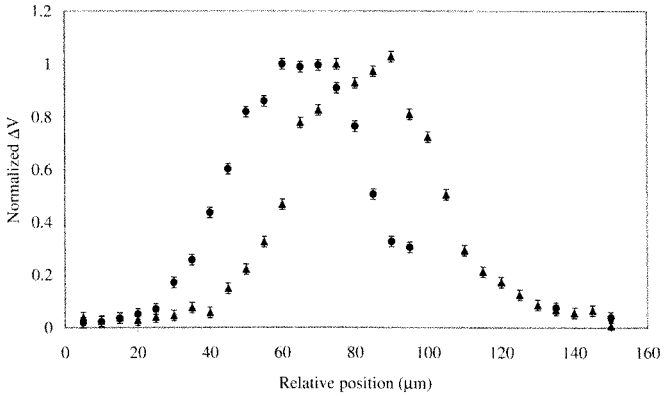


Fig. 12. Parallel readout of two RADFETs on one chip shows a different peak dose position. The difference indicates a misalignment of the RADFETs relative to the microbeam. This is a useful indication of the degree of misalignment and also demonstrates the possibility of making high spatial resolution measurement.

of the relative dose profile in the pulsed synchrotron radiation microbeam (as in Fig. 12) using an advanced readout system, a multiple integrated RADFET, and a computer-controlled goniometer was achieved in a time of 1 min only.

Further relative dose distributions should now be compared with GaF film measurements. It should then be a minor step to obtain the absolute calibration of the beam profile. Other investigations desirable are the understanding of the effect of oxide thickness on the spatial resolution and selection and fabrication of devices carrying the best values and best number of RADFETs per chip.

## V. Conclusion

The first online scanning MOSFET dosimetry system with high spatial resolution has been developed and tested in several situations, including penumbras, radiation leakages, and radiation microbeams. Very steep dose gradients are measured rapidly by scanning machinery and PC-controlled readout. In routine therapy machines, a penumbra of width 100 $\mu$m can be profiled with simple equipment. The leakage of radiation leakage through a "closed" multileaved collimator, used for high-energy intensity-modulated therapy, has been profiled. The results were in excellent agreement with GaF film and were obtained much more promptly and in a computerized form. A key to this ease of profiling was the online MOSFET dosimetry system developed by the Centre for Medical Radiation Physics, University of Wollongong, Australia. The system takes into account the advantages of integrated MOSFET dosimeters (real-time remote readout, sensors separated by small dimensions) and corrects for the disadvantages (such as temperature dependence and drift effects due to total dose).

In advanced synchrotron X-ray microbeam systems, the ability to make automatically profiles of 30-$\mu$m-wide beams and to achieve micrometer spatial resolution was also demonstrated. Here, the use of oxide film only 1 $\mu$m thick (or less) in the "edge-on" orientation opens up a large range of possibilities in micrometer-scale profiling of photon and particle beam spots. Preliminary results demonstrated that these ideas are suitable for clinical practice and are intriguing scientifically. Further

work is needed in the areas of absolute calibration and ideal oxide film arrangements and advanced silicon-based device structures for the profiling of small radiation fields. The overall MOSFET dosimetry system as described will offer savings of time and improvement of outcomes in intensity-modulated and conformal radiotherapy.

## ACKNOWLEDGMENT

The authors would like to thank P. Ihnat of the CMRP for his electronics support in the reader development and S. Bazley, Mater Hospital, for his support with the software development of MosPlot 4.1 and the experiments involving the LINAC. They would also like to thank the technical staff at ESRF for their help during the experiments at ESRF.

## REFERENCES

[1] S. Buchner and A. B. Campbell *et al.*, "Investigation of single-ion multiple-bit upsets in memories on board a space experiment," *IEEE Trans. Nucl. Sci.*, vol. 47, pp. 705–711, 2000.

[2] J. L. Autran, P. Masson, N. Freud, C. Raynaud, and C. Riekel, "Micro irradiation experiments in MOS transistor using synchrotron radiation," *IEEE Trans. Nucl. Sci.*, vol. 47, pp. 574–579, 2000.

[3] A. Rosenfeld, G. Kaplan, B. Allen, A. Dilmanian, and A. Holmes-Siedle, "MOSFET dosimetry of X-ray microbeams," *IEEE Trans. Nucl. Sci.*, vol. 46, pp. 1774–1780, 1999.

[4] A. Holmes-Siedle and L. Adams, *Handbook of Radiation Effects*, 2nd ed. Oxford, U.K.: Oxford Univ. Press, 2001.

[5] ——, "RADFETs: A review of the use of metal–oxide–silicon devices as integrating dosimeters," *Radiat. Phys. Chem.*, vol. 28, no. 2, pp. 235–244, 1986.

[6] J. A. Laissue *et al.*, "Neuropathology of ablation of rat gliosarcomas and contiguous brain tissue using a microplanar beam of synchrotron-wiggler-generated X-rays," *Int. J. Cancer*, vol. 78, pp. 654–660, 1998.

[7] J. A. Laissue *et al.*, "Microbeam radiation therapy," in *Proc. SPIE Conf. Medical Applications of Penetrating Radiation*, vol. 3770, Denver, CO, July 1999.

[8] D. N. Slatkin *et al.*, "Microbeam radiation therapy," *Med. Phys.*, vol. 19, pp. 1395–1400, 1992.

[9] D. W. Archer, "Collimator for producing an array of microbeams," US Patent 5 771 270, June 23, 1998.

[10] J. Chang, G. S. Mageras, C. S. Chui, C. C. Ling, and W. Lutz, "Relative profile and dose verification of intensity-modulated radiation therapy," *Int. J. Radiat. Oncol. Biol. Phys.*, vol. 47, no. N1, pp. 231–240, 2000.

[11] K. E. Duftschmid, P. Kindl, B. Obenaus, Ch. Strachotinsky, and N. Winker, "Precision dosimetry in narrow collimated radiation beams of the Leksel Gamma Knife," *Rad. Prot. Dosim.*, vol. 66, no. N1–4, pp. 295–298, 1996.

[12] A. Holmes-Siedle, *REM's Integrating Dosimeter Based on the RADFET: An Introduction*. Eynsham, U.K.: REM Oxford, 2001.

[13] Z. Savic, B. Rajdenovic, M. Pejovic, and N. Stojadinivic, "The contribution of border traps to the threshold voltage shift in pMOS dosimetric transistors," *IEEE Trans. Nucl. Sci.*, vol. 42, pp. 1445–1453, 1995.

[14] M. Soubra, J. Cygler, G. Mackay, I. Thompson, and A. Ribes, "Evaluation of dual bias, dual metal oxide silicon semiconductor field effect transistor detector as radiation dosimeters," *Med. Phys.*, vol. 21, pp. 567–572, 1994.

[15] M. G. Buehler, B. R. Blaes, G. A. Soli, and G. R. Tardio, "On-chip, p-MOSFET dosimetry," *IEEE Trans. Nucl. Sci.*, vol. 40, pp. 1442–1449, Dec. 1993.

[16] T. LoSasso, C. Chui, and C. Ling, "Physical and dosimetric aspects of a multileaf collimation system used in the dynamic mode for implementing intensity modulated radiotherapy," *Med. Phys.*, vol. 25, pp. 1919–1927, 1998.

[17] I. Orion, A. B. Rosenfeld, F. A. Dilmanian, F. Telang, B. Ren, and Y. Namito, "Monte Carlo simulations of dose distribution form a synchrotron-produced micro-planar beam array using the EGS4 code system," *Med. Phys. Biol.*, vol. 45, pp. 2497–2508, 2000.